Conformational Analysis of Mitochondrial and Microsomal Cytochrome P-450 by Resonance Raman Spectroscopy

Peter Hildebrandt,*,‡ George Heibel,‡ Pavel Anzenbacher,§ Reinhard Lange,∥ Volker Krüger,⊥ and Anton Stier⊥

Max-Planck-Institut für Strahlenchemie, D-45470 Mülheim, Federal Republic of Germany, Institute of Experimental Biopharmacy, Pro. Med. CS-Czech Academy of Sciences, Hradec Králové, Czech Republic, Institut National de la Santé et de la Recherche Médicale, Unité 128, Montpellier, France, and Max-Planck-Institut für Biophysikalische Chemie, D-37077 Göttingen, Federal Republic of Germany

Received April 25, 1994; Revised Manuscript Received July 11, 1994®

ABSTRACT: Mitochondrial and microsomal cytochromes P-450$_{SCC}$ and P-450$_{LM2}$ in the ferric substrate-free and substrate-bound states were studied by resonance Raman spectroscopy. In the spectra of cytochrome P-450$_{SCC}$ two conformational states (A and B) were detected, each of them constituting an equilibrium between a six-coordinated low-spin and a high-spin form. Both the conformational and the spin equilibria are pH- and temperature-dependent, which is in line with previously published results [Lange, R., Larroque, C., & Anzenbacher, P. (1992) *Eur. J. Biochem. 207*, 69–73)]. On the basis of well-resolved resonance Raman spectra, measured at different pH and temperatures, these equilibria were analyzed quantitatively. Both low-spin configurations of A and B exhibit different band patterns in the spin state marker band region, indicating differences in the active-site structures. While in the high-spin configuration of state A the heme iron remains weakly bound by a sixth ligand, the high-spin form of state B is five-coordinated. Binding of cholesterol to cytochrome P-450$_{SCC}$ causes a significant population of the high-spin forms, particularly of state A (62%). On the other hand, binding of 22*R*-hydroxycholesterol to the substrate-free enzyme leaves the overall spin equilibrium largely unchanged, i.e., six-coordinated low spin (76% A and 24% B). In both substrate-bound complexes, interactions between the substrate and the heme lead to small but distinct differences in the resonance Raman spectra of the low-spin form of state A. In contrast to cytochrome P-450$_{SCC}$, the resonance Raman spectra of microsomal cytochrome P-450$_{LM2}$ provide no indications for multiple conformers at 22 °C. Binding of benzphetamine causes a partial conversion from the six-coordinated low-spin to a high-spin state (28%) in which a sixth ligand may still weakly interact with the heme iron, similar to the case of the HS species of state A in cytochrome P-450$_{SCC}$. The comparison of the results obtained for both enzymes indicate that at ambient temperature the protein structure, at least in the heme pocket and the substrate binding site, is significantly more flexible in cytochrome P-450$_{SCC}$. This conformational flexibility may be related to the ability to bind the sterically demanding natural substrates and may control the product specificity of the catalytic process.

Cytochromes P-450 catalyze the oxygenation of a variety of exogenous and endogenous compounds (Ruckpaul & Rein, 1984; Ortiz de Montellano, 1986; Schuster, 1989). The active site of these enzymes is an iron protoporphyrin IX axially coordinated by a cysteine thiolate (Raag & Poulos, 1992). In the resting (ferric) state of the enzyme, the second axial position, which is located in close proximity to the substrate binding site, is either vacant or temporarily occupied by a weak field ligand such as a water molecule and serves as the dioxygen binding site during the catalytic process. The individual steps of the reaction cycle, i.e., substrate binding, electron transfer, and oxygen binding, are intimately connected with changes of coordination pattern and the spin configuration of the heme iron, which in turn are suggested to be of functional relevance for the enzymatic process (Rein et al., 1984; Backes et al., 1985; Sligar & Gunsalus, 1979). Thus, it is of particular interest to analyze the parameters which control the spin and coordination configuration of the heme. In this work, we have focused on the first step of the reaction cycle, i.e., the substrate binding to the ferric enzyme, comparing the qualitatively different response of two representatives of the cytochrome P-450 family: microsomal cytochrome P-450$_{LM2}$ (LM2)[1] and mitochondrial cholesterol-side-chain-cleaving cytochrome P-450$_{SCC}$ (SCC) (Ruckpaul & Rein, 1984; Ortiz de Montellano, 1986; Schuster, 1989).

Substrate-binding to LM2, which has been extensively studied by a variety of techniques, leads to a conversion from a six-coordinated low-spin (6cLS) configuration to a high-spin form (HS), the degree of the conversion depending on the kind of the substrate (Cinti et al., 1979; Rein et al., 1984; Hildebrandt et al., 1989a,b). These spin state changes can readily be attributed to a simple two-state equilibrium. In contrast, SCC reveals a more complex behavior. Previous thermodynamic investigation of SCC led to a reaction model comprising a temperature-dependent equilibrium between two protein conformers A and B (Lange et al., 1992a). Both species exist in a pH-dependent spin equilibrium between a high-spin

* Address correspondence to this author at the Max-Planck-Institut für Strahlenchemie, Stifstr. 34-36, D-45470 Mülheim, FRG.
‡ Max-Planck-Institut für Strahlenchemie.
§ Pro. Med. CS-Czech Academy of Sciences.
∥ Institut National de la Santé et de la Recherche Médicale.
⊥ Max-Planck-Institut für Biophysikalische Chemie.
® Abstract published in *Advance ACS Abstracts,* October 1, 1994.

[1] Abbreviations: SCC, cholesterol-side-chain-cleaving cytochrome P-450, cholesterol monooxygenase = CYP11A1; LM2, liver microsomal cytochrome P-450 isozyme 2 = CYP2B4; CAM, cytochrome P-450 (camphor-5-*exo*-hydroxylase) from *Pseudomonas putida* = CYP101; BM-3, heme protein domain fatty acid monooxygenase cytochrome P-450 BM-3 from *Bacillus megaterium* = CYP102 [for the enzyme nomenclature, see Nelson et al. (1993); all abbreviations refer to the ferric state of the enzymes; the substrate-free forms are denoted by the superscript 0; the substrates bound to the enzymes are given in parentheses]; chol, cholesterol; 22R, 22*R*-hydroxycholesterol; BP, benzphetamine; PPIX, ferric protoporphyrin IX; RR, resonance Raman; 6cLS, six-coordinated low-spin; 6cHS, six-coordinated high-spin; 5cHS, five-coordinated high-spin.

0006-2960/94/0433-12920$04.50/0

and a low-spin form which can be summarized according to the following reaction scheme:

$$HS_A \rightleftarrows LS(H^+)_A \rightleftarrows LS_A \rightleftarrows LS_B \rightleftarrows LS(H^+)_B \rightleftarrows HS_B \quad (1)$$

The conformational state A prevails at low temperature and low pH and is converted to state B upon increasing temperature or pH. This model was confirmed by analyzing the kinetics of the conformational transitions following rapid pH jumps as well as by circular dichroism (CD) experiments (Lange et al., 1992b). The spectroscopic data revealed that in state A the helical content of the protein is slightly increased and the polarity of the tyrosine environment is higher than in state B. These protein conformational changes depend on the presence of biological effector molecules such as specific substrates or adrenoxine, which are known to affect the active site of the enzyme, i.e., the heme pocket.

Resonance Raman (RR) spectroscopy is a particularly powerful tool for studying the structure of the heme and its interactions with the protein environment (Spiro, 1988). It has successfully been employed for investigating heme proteins including cytochromes P-450 (Spiro, 1988; Hildebrandt, 1992). On the basis of a large body of experimental data, empirical relationships have been established between vibrational frequencies and structural parameters of the heme. In this way it was found that the core size of the porphyrin, which in turn depends on the oxidation, spin, and ligation state of the metal ion, is correlated with the frequencies of most of the porphyrin modes above 1450 cm^{-1}, the so-called spin marker bands (Partharasathi et al., 1987; Kitagawa & Ozaki, 1987). Hence, RR spectroscopy holds promise to contribute to the elucidation of the spin equilibria in cytochromes P-450. In this work, we have employed to this technique for a comparative study of SCC and LM2 in order to gain more insight into structural specificity of the active sites of both enzymes.

MATERIALS AND METHODS

Sample Preparation. SCC was isolated from beef adrenal cortex mitochondria as described elsewhere (Lange et al., 1988). The purified SCC contained one or two molecules of cholesterol (chol), i.e., SCC(chol) (Suhara et al., 1978; Lange et al., 1988). Removal of the bound cholesterol was achieved according to the procedure described by Larroque and Van Lier (1986). The endogeneous cholesterol was enzymatically converted to pregnenolone, which was dissociated from SCC on an adrenodoxin–Sepharose column. Adrenoxin and adrenoxine reductase were prepared according to Suhara et al. (1972a,b). The enzyme was dissolved in 50 mM phosphate buffer adjusted to pH 7.4 unless indicated otherwise. The isozyme LM2 was isolated and purified from liver microsomes of phenobarbital-treated rabbits (Imai et al., 1980). Oligomers of LM2 were prepared according to the procedure described by Hildebrandt et al. (1989b). The enzyme was dissolved in a solution containing 20% (by volume) glycerol and 150 mM phosphate (pH 7.25). For the RR experiments, the concentration of the enzymes was 10 μM. Binding of exogenous substrates (>95%) was achieved by addition of 20 μM 22*R*-hydroxycholesterol (22R) to SCC [SCC(22R)] and 4 mM benzphetamine to LM2 [LM2(BP)] (Lange et al., 1992a; Hildebrandt et al., 1989b). Benzphetamine was prepared as described elsewhere (Heinzelmann & Aspergren, 1957). 22*R*-hydroxycholesterol was purchased from Sigma. All other chemicals were of the highest commercially available quality.

Resonance Raman Measurements. The RR spectra were measured with 413-nm excitation using a scanning double monochromator with a spectral resolution of 2.8 cm^{-1} and a step width of 0.2 cm^{-1}. Details of the equipment are described elsewhere (Heibel et al., 1993). All spectra were recorded by repetitive scanning. The samples were contained in a rotating cuvette to avoid laser-induced degradation of the enzymes. For low-temperature measurements the cuvette was deposited in a home-built thermostated chamber. LM2 was perfectly stable during the RR experiments for 8 h. Slow time-dependent spectral changes, however, were noted for SCC. Thus, we had to replace the samples by fresh ones after about 2 and 3 h for measurements at pH 8.4 and 7.4, respectively. Such spectral changes did not correspond to the formation of P-420, as checked by absorption spectroscopy after the RR experiment.

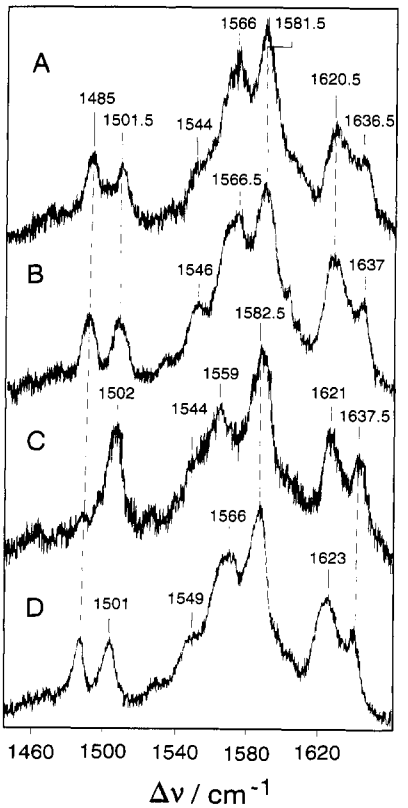

FIGURE 1: High-frequency RR spectra of the cholesterol-bound SCC at various pH values and temperatures. (A) pH = 7.4, T = 22 °C; (B) pH = 7.4, T = 4 °C; (C) pH = 8.4, T = 22 °C; (D) same as (A) but in the presence of 10% (v/v) glycerol.

The RR measurements of SCC were hampered by the strong fluorescence background. This background was removed from the RR spectra by polynomial subtraction. In addition, the Raman bands of glycerol were subtracted. The RR spectra obtained in this way were analyzed by a band-fitting program as described elsewhere (Heibel et al., 1993).

RESULTS

Analysis of the RR Spectra of Cytochrome P-450 SCC. The RR spectra of SCC(chol) measured at various pH values and temperatures are shown in Figure 1. The spectra display the region of the spin state marker bands, the frequencies of which are correlated with the spin and ligation states of the heme iron (Partharasathi et al., 1987). On the basis of these relationships, the mode ν_3 is expected at ~1480, 1490, and 1500 cm^{-1} for a 6cHS, 5cHS, and 6cLS ferric heme, respectively.[2] This mode is well separated from other porphyrin modes and, hence, most appropriate to determine

[2] The mode numbering refers to Abe et al. (1978).

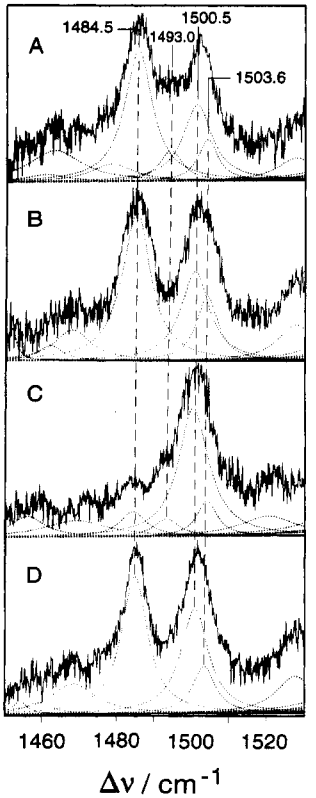

FIGURE 2: RR spectra of the cholesterol-bound SCC at various pH values and temperatures in the ν_3 band region. (A) pH = 7.4, T = 22 °C; (B) pH = 7.4, T = 4 °C; (C) pH = 8.4, T = 22 °C; (D) same as (A) but in the presence of 10% (v/v) glycerol. The dotted lines represent the fitted Lorentzian line shapes.

the spin and coordination configuration. At pH 7.4, the RR spectra reveal a distinct band at ~1485 cm^{-1} (Figure 1A,B,D), which is readily attributed to a HS configuration. The frequency is located just between the expected values for 5cHS and 6cHS configurations (Partharasathi et al., 1987) so that the determination of the coordination number solely based on this band is not unambiguous. Adjacent to this band, we note a peak at ~1501 cm^{-1}, characteristic for 6cLS state. However, this latter peak is clearly asymmetric, suggesting that it includes two components. In addition, the room-temperature RR spectrum at pH 7.4 (Figure 1A) reveals an appreciable RR intensity between the 1484-cm^{-1} and 1501-cm^{-1} peaks at ~1493 cm^{-1}, which would correspond to a 5cHS species. These qualitative considerations are confirmed by a more detailed investigation of the ν_3 band region as demonstrated in Figure 2. The band-fitting analysis yields four bands at 1484.5 (HS), 1493.0 (5cHS), 1500.5 (6cLS), and 1503.6 cm^{-1} (6cLS) with different relative intensities in the four spectra. These results are in line with previous findings by Lange et al. (1992a,b) who found that SCC exists in a conformational equilibrium between two conformers and each of these conformers constitutes a pH- and temperature-dependent spin equilibrium. The four species not only differ with respect to the mode ν_3 but also should exhibit different frequencies for the remaining modes in the marker band region (1400–1660 cm^{-1}), leading to the broad and complex vibrational band pattern as shown in Figure 1.

In an attempt to disentangle these spectra, we assumed that the spectral parameters (frequencies, half-widths, relative intensities) of the individual species do not depend on the pH or temperature. This implies that the measured RR spectra can be simulated by a weighted set of four component spectra. The spectral parameters of these spectra and the weighting factors were determined in an iterative way. At first, we have removed the content of the 5cHS species, which is only present in the room-temperature spectra at pH 7.4 (Figures 1A and 2A) and pH 8.4 (Figures 1C and 2C). Even in these spectra the contribution of this form is relatively low with respect to other species so that, in a first approximation, all other modes of the 5cHS form except the ν_3 mode can be neglected. Hence, we subtracted only the ν_3 band at 1493 cm^{-1} by using the line shapes as calculated in Figure 2A,C. The resultant spectra and the spectra in Figure 1B,D were then used to construct crude spectra of the HS form, which is characterized by the 1484-cm^{-1} band, and the two 6cLS forms (1500- and 1503-cm^{-1} bands) by mutual subtraction using the ν_3 bands as a reference as determined in Figure 2. The difference spectra obtained in this way were analyzed by band-fitting analysis, yielding approximate spectral parameters for the HS and the two 6cLS species. In the second step we have used these data as the starting set of parameters in the band-fitting analysis of the raw spectra. Initially, the spectral parameters of the individual species were kept constant, trying to simulate the spectra as a superposition of these component spectra. Then, the spectral parameters were progressively released to optimize the fits [cf. Hildebrandt et al. (1990)]. Thus, for each species and for each raw spectrum modified, spectral parameters were obtained which were averaged and used as a new initial set of parameters to fit the raw spectra again. This procedure was repeated about 8 times until a consistent fit of the measured spectra in Figure 1 was achieved with the same frequencies (±0.4 cm^{-1}), half-widths (±0.4 cm^{-1}), and relative intensities of the various modes (±15%) for each given species. The spectral parameters obtained in this way are listed in Table 1. The band assignment has been discussed in detail elsewhere (Anzenbacher et al., 1989; Hildebrandt et al., 1989a,b; Hildebrandt, 1992).

The relative contributions of the four species to the RR spectra in Figure 1 were determined from the average RR intensity I_{av}, which is the average of the RR intensities of all individual modes n of a given species according to

Table 1: Spectral Parameters of SCC and LM2 in the Marker Band Region[a]

	SCC					LM2
	cholesterol			22R	substrate-free	substrate-free
mode	HS	6cLS	6cLS	6cLS	6cLS	6cLS
ν_3	1484.5	1503.6	1500.5	1500.1	1500.3	1501.4
	(8.9)	(7.4)	(9.3)	(8.5)	(9.2)	(10.2)
	1.00	*1.00*	*1.00*	*1.00*	*1.00*	*1.00*
ν_{38}	1527.5	1543.8	1545.5	1548.2	1550.0	1549.1
	(12.2)	(11.4)	(16.9)	(16.9)	(8.7)	(16.4)
	0.24	*1.29*	*0.43*	*0.40*	*0.32*	*0.56*
ν_{11}	1560.9	1564.2	1558.2	1558.5	1557.6	1562.3
	(15.3)	(11.8)	(12.4)	(9.2)	(7.9)	(13.4)
	0.73	*0.96*	*0.84*	*0.90*	*0.67*	*0.66*
ν_2	1568.0	1580.5	1582.8	1582.7	1581.7	1581.5
	(12.4)	(15.7)	(16.1)	(16.1)	(13.2)	(14.7)
	0.90	*2.04*	*1.23*	*1.98*	*1.83*	*1.76*
ν_{37}	1583.2	1595.5	1601.4	1601.6	1602.2	1603.8
	(14.9)	(5.9)	(7.7)	(6.2)	(6.4)	(10.6)
	1.14	*1.03*	*0.28*	*0.36*	*0.53*	*0.72*
ν_{10}	1602.9	1637.3	1638.7	1637.6	1636.9	1638.2
	(5.7)	(8.2)	(8.1)	(9.5)	(12.0)	(11.4)
	0.11	*1.19*	*0.59*	*0.69*	*0.52*	*0.74*
	1620.7	1621.3	1617.5	1616.9	1618.6	1620.5
	(15.3)	(14.1)	(5.5)	(5.2)	(6.8)	(8.9)
$\nu_{C=C}$	*0.55*	*2.31*	*0.36*	*0.38*	*0.37*	*1.00*
	1630.5	1631.8	1629.5	1627.9	1627.3	1628.7
	(7.7)	(6.2)	(11.4)	(6.7)	(10.9)	(13.2)
	0.10	*0.36*	*0.48*	*0.47*	*0.49*	*0.50*

[a] The frequencies and half-widths (in parentheses) are given in centimeters^{-1}; the relative intensities (in italics) refer to the mode ν_3. The mode numbering follows the notation by Abe et al. (1978).

$$I_{av} = \sum_n \frac{I(\nu_n)/R(\nu_n)}{n} \quad (2)$$

where $R(\nu_n)$ is the intensity ratio of the mode n to the reference mode ν_3, obtained from the data in Table 1, and $I(\nu_n)$ is the actual intensity of this mode in the measured RR spectrum.

Assignment of the RR Spectra to Different Conformers of SCC. The average intensity data, which are listed in Table 2, can now be used to determine the weighting factors to construct the pure spectra of the major HS and the two 6cLS forms by mutual subtraction of the four RR spectra of SCC from Figure 1. The difference spectra obtained in this way are displayed in Figure 3.

Now we wish to assign the four species detected by RR spectroscopy to the HS and LS forms of the two conformational states of SCC(chol) previously found by Lange et al. (1992a,b). According to the model suggested by these authors, both states—denoted as A and B—are linked by a pH-dependent equilibrium according to

$$L' = \frac{c_{LS(B)} c_{H^+}^{\Delta m}}{c_{LS(A)}} \quad (3)$$

where Δm is net change of the number of bound protons during the transformation between A and B. $c_{LS(A)}$ and $c_{LS(B)}$ are the concentrations of the LS forms of A and B, which are related to the RR intensities I_i of a given mode according to

$$c_i = f_i I_i \quad (4)$$

where f_i is a constant which is proportional to the Raman cross section. After combining eqs 3 and 4, one obtains a constant R_{H^+} for two different pH values, 7.4 and 8.4, (T = 22 °C):

$$R_{H^+} = \frac{c_{H^+}^{\Delta m}(\text{pH } 8.4)}{c_{H^+}^{\Delta m}(\text{pH } 7.4)} = \frac{I_{LS(B)}(\text{pH } 7.4) I_{LS(A)}(\text{pH } 8.4)}{I_{LS(B)}(\text{pH } 8.4) I_{LS(A)}(\text{pH } 7.4)} \quad (5)$$

With Δm = –0.3 (Lange et al., 1992a), R_{H^+} is calculated to 1.99. From the corresponding values of the RR intensities for both LS forms in Table 2, it can readily be verified that the 6cLS species exhibiting the ν_3 bands at 1500.5 and 1503.6 cm^{-1} must be assigned to the LS forms of state A and B, respectively.

In order to reach an unambiguous assignment of the HS configurations to the states A and B, further themodynamic data of the SCC(chol) have to be taken into account. Lange et al. (1992a,b) determined the spin equilibrium contstants K_s as defined according to

$$K_s = \frac{c_{HS(A)} + c_{HS(B)}}{c_{6LS(A)} + c_{6cLS(B)}} = \frac{f_{5cHS} I_{5cHS} + f_{HS} I_{HS}}{f_{6cLS(A)} I_{6cLS(A)} + f_{6cLS(B)} I_{6cLS(B)}} \quad (6)$$

for pH 7.4 and 8.4 (each at T = 22 °C) and for pH 7.4 at 4 °C. Furthermore, the thermodynamic analysis has revealed that the spin equilibrium of state B decreases upon increasing the pH and the conformational equilibrium is shifted toward state B with increasing pH and temperature. Using these constraints, we varied the proportionality factors f_i until a satisfactory fit of the four spin equilibria as defined by eq 6 to the corresponding RR intensity data in Table 2 was achieved. In this way it turned out that a reasonable fit with a standard deviation of less than 20% was only possible by assigning the 5cHS (ν_3 = 1493.0 cm^{-1}) and the HS species (ν_3 = 1484.5 cm^{-1}) to the states B and A, respectively.

Table 2: Relative RR Intensities (ν_3) of the Various Species of SCC(chol)[a]

species	T = 22 °C, pH 7.4	T = 4 °C, pH 7.4	T = 22 °C, pH = 7.4, glycerol	T = 22 °C, pH 8.4
5cHS	238			142
HS	1000	1000	1000	202
6cLS(1500)	627	600	722	1000
6cLS(1503)	329	471	321	258

[a] The RR intensities are average values according to eq 2 and normalized with respect to the strongest component in each spectrum.

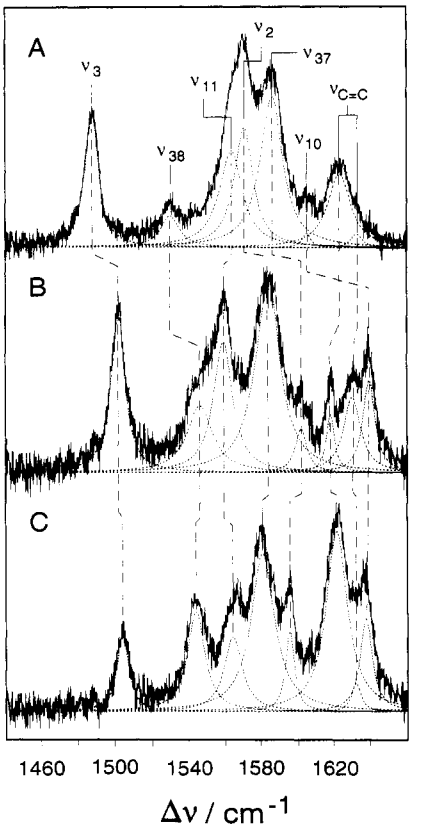

FIGURE 3: High-frequency RR spectra of the HS and 6cLS forms of the cholesterol-bound SCC. (A) HS (conformer A); (B) 6cLS (conformer A); (C) 6cLS conformer (B). The spectra were obtained by a subtraction procedure as described in the text. The dotted lines represent the fitted Lorentzian line shapes.

Table 3: Relative Concentrations of the Various Conformational and Spin States of SCC[a]

	cholesterol					
	pH 7.4					
species	T = 22 °C	T = 4 °C	T = 22 °C, glycerol	pH 8.4 T = 22 °C	22R pH 7.4 T = 4 °C	substrate-free pH 7.4 T = 22 °C
A, 6cLS	0.17	0.16	0.20	0.49	0.76	0.71
A, HS	0.62	0.64	0.66	0.23	0.0	0.03
B, 6cLS	0.13	0.20	0.14	0.19	0.24	0.21
B, 5cHS	0.08	0.0	0.0	0.09	0.0	0.04

[a] The concentrations were calculated according to eq 7 with $f_{5cHS(B)}$ = 0.571, $f_{HS(A)}$ = 1.000, $f_{6cLS(A)}$ = 0.424, and $f_{6cLS(B)}$ = 0.643.

The resultant f_i values, which are included in Table 3, can now be used to determine the relative concentrations of the various species c_i according to

$$c_i = \frac{f_i I_{av,i}}{\sum_i f_i I_{av,i}} \quad (7)$$

Table 4: Equilibrium Constants of SCC

system		thermodynamic constants UV–vis[a]	RR[b]
total spin equilibrium	T = 22 °C, pH = 7.4	2.3	2.38
	T = 4 °C, pH = 7.4	2.2	1.80
	T = 22 °C, pH = 8.4	0.95	0.48
spin equilibrium state B	T = 22 °C, pH = 7.4	0.4[c]	0.64
	T = 22 °C, pH = 8.4	<0.1[c]	0.49
conformational equilibria between states A and B	K_{con}(4 °C)/K_{con}(22 °C, pH 7)	>1	1.14
	K_{con}(pH 8)/K_{con}(22 °C, pH 7)	<1	0.70
	K_{con}(glycerol)/K_{con}(22 °C, pH 7)	>1	1.74

[a] Calculated from UV–vis spectroscopic experiments by Lange et al. (1992a). [b] Determined from the relative concentrations in Table 3 obtained from the RR data as described in the text. [c] Determined for SCC in 35% ethylene glycol.

where $I_{av,i}$ are the RR intensities listed in Table 3. The relative concentrations obtained in this way are given in Table 3 and equilibrium constants calculated from these data are listed in Table 4. The comparison of these data with those obtained by UV–vis spectroscopic experiments by Lange et al. (1992a) reveals a satisfactory agreement. The relatively large discrepancy for the spin equilibrium constant at pH 8.4 may partly be due to the lower accuracy of the intensity determination for the weak HS marker bands. The spin equilibrium constants of state B as determined from the RR experiments are larger than the values reported by Lange et al. (1992a), who have determined these constants for SCC dissolved in 35% ethylene glycol. Presumably, polyalcohols such as glycerol or ethylene glycol shift the spin equilibrium of state B toward the 6cLS form as suggested by the present RR results (Table 3), so that the spin equilibrium constants are smaller than in purely aqueous solutions.

The RR spectra of the substrate-free SCC (SCC^0) and the 22*R*-hydroxycholesterol-bound SCC [SCC(22R)] are shown in Figure 4. In the first step of the band fitting we have analyzed the ν_3 band region using the same spectral parameters as determined for the four spin and coordination states of SCC(chol). It was found that in both spectra the 1500-cm^{-1} band (6cLS, A) clearly prevails, while the 1503-cm^{-1} band (6cLS, B) gives a significantly smaller contribution to the ν_3 envelope. The HS forms are very weak in SCC^0 and could not be detected at all in SCC(22R). In the second step we tried to simulate the entire spectral range as displayed in Figure 4 by a simple superposition of the spectra of the various components of SCC(chol), starting with weighting factors determined from the ν_3 band analysis. However, in this way no satisfactory fit could be obtained. This implies that either the "four-species" model that can sufficiently account for the RR spectra of SCC(chol) fails in the case of SCC^0 and SCC(22R), or, more likely, the removal of cholesterol or the replacement by 22*R*-hydroxycholesterol affects the spectral parameters of the various species of SCC. Unfortunately, the RR spectra in Figure 4 alone are sufficient to determine such effects for each of the four species. For the minor components, i.e, the 6cLS(B) and the two HS forms, even drastic variations of the spectral parameters only moderately improved the simulations of both spectra. Hence, we have optimized the fits by exclusively varying the spectral parameters of the prevailing form, i.e., 6cLS(A), while those of the other species were kept constant. The resultant simulations are shown in Figure 4 and the modified spectral parameters of the 6cLS(A) species are listed in Table 1. The relative concentrations of the various species were determined as described above (Table 3), assuming that the f_i values (eq 7) are the same as in SCC(chol).

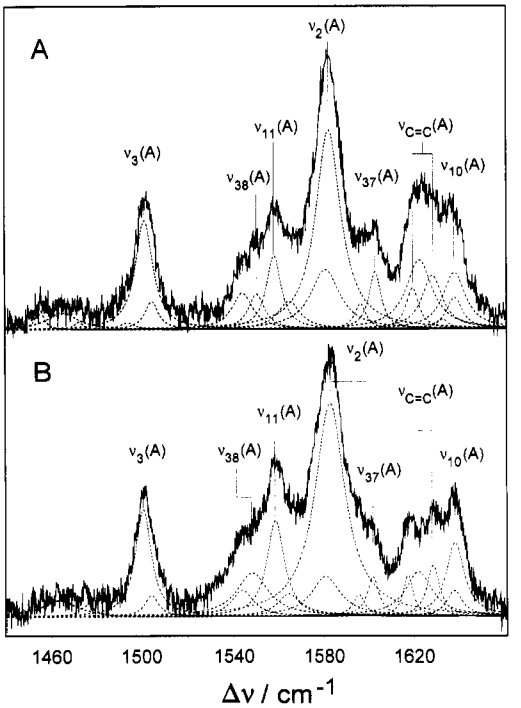

FIGURE 4: High-frequency RR spectra of the substrate-free SCC (A) and the 22*R*-hydroxycholesterol-bound SCC (B). The spectra were measured at pH 7.4 at 22 °C (A) and at 4 °C (B). The dotted lines represent the fitted Lorentzian line shapes obtained as described in the text. The band components labeled A refer to the 6cLS form of state A; the remaining band components refer to the 6cLS form of state B and the HS forms.

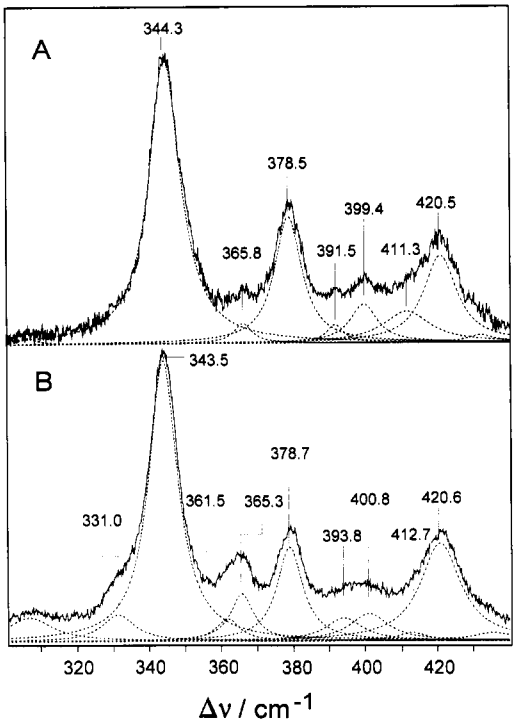

FIGURE 5: Low-frequency RR spectra of SCC. (A) Cholesterol-bound SCC; (B) 22*R*-hydroxycholesterol-bound SCC. The spectra were measured at 4 °C and pH 7.4. The dotted lines represent the fitted Lorentzian line shapes.

Figure 5 shows the low-frequency RR spectra of SCC(chol) and SCC(22R), both measured at pH 7.4 and at 4 °C. The spectra display far-reaching similarities and the band-fitting analysis in fact reveals only small changes of the spectral parameters of the bands upon replacement of cholesterol by 22*R*-hydroxycholesterol (Table 5). On first sight, this finding is quite surprising since the exchange of the substrates is

Table 5: Spectral Parameters of SCC and LM2 in the Low-Frequency Region[a]

SCC		LM2	
cholesterol	22*R*-hydroxycholesterol	substrate-free	benzphetamine
306.0 (6.0) *0.02*	306.3 (15.9) *0.08*	301.5 (13.7) *0.08*	302.4 (14.3) *0.09*
		308.2 (8.7) *0.07*	310.4 (8.8) *0.07*
	331.0 (11.0) *0.09*	328.6 (12.9) *0.08*	330.2 (15.2) *0.12*
		339.1 (15.5) *0.15*	342.7 (15.5) *0.25*
344.3 (10.5) *1.00*	343.5 (9.6) *1.00*	346.7 (10.3) *1.00*	346.8 (9.5) *1.00*
	361.4 (8.0) *0.08*		
365.8 (6.2) *0.07*	365.3 (8.0) *0.17*	367.8 (7.2) *0.06*	369.9 (7.5) *0.04*
378.5 (9.1) *0.45*	378.7 (8.7) *0.33*	380.5 (9.9) *0.61*	380.0 (9.8) *0.64*
391.5 (5.9) *0.06*	393.8 (12.4) *0.08*	390.5 (7.9) *0.10*	390.7 (10.1) *0.13*
399.4 (9.2) *0.14*	400.8 (12.8) *0.10*	397.6 (10.4) *0.08*	397.4 (11.9) *0.09*
		404.4 (14.1) *0.10*	405.1 (15.2) *0.16*
411.3 (15.7) *0.11*	412.7 (9.6) *0.03*	415.9 (15.3) *0.26*	415.5 (13.8) *0.25*
420.6 (11.1) *0.31*	420.5 (13.5) *0.35*	422.3 (10.6) *0.24*	421.4 (12.7) *0.31*
431.7 (8.7) *0.03*	435.2 (14.2) *0.03*	430.1 (14.2) *0.08*	428.4 (16.2) *0.16*

[a] The frequencies and half-widths (in parentheses) are given in centimeters^{-1}; the relative intensities (in italics) refer to the band at ~345 cm^{-1}.

associated with a drastic shift of the spin equilibrium toward the LS forms. This implies that the low-frequency bands of the HS forms are relatively weak compared to those of the LS species. The most remarkable differences between both spectra are a frequency downshift of the band at 344.3 cm^{-1} and upshifts of the bands at 391.5, 39.4, and 411.3 cm^{-1} by 1–2 cm^{-1} upon binding of 22R, accompanied by a broadening of most of the bands. Since the ratio between the 6cLS(A) and 6cLS(B) form increases from 0.8 in SCC(chol) to 3.2 in SCC(22R) (Table 3), it is evident that the low-frequency bands of both 6cLS forms are at very similar positions so that they cannot be separated by the band-fitting analysis. Hence, a change of the ratio of both 6cLS configurations is reflected by shifts of the maxima and a broadening of the unresolved peaks.

In addition to these changes, there are two weak but distinct new bands at 331.0 and 361.4 cm^{-1} in SCC(22R). These bands cannot be detected in SCC(chol). Thus it is ruled out that these bands are an intrinsic property of the conformational state A. Instead they may reflect the specific interactions between 22R and the heme pocket.

Analysis of the RR Spectra of Cytochrome P-450 LM2. The RR spectra of the oligomeric LM2 are shown in Figures 6 and 7. In the region of the spin state marker bands (Figure 6), the spectrum of the substrate-free LM2 (LM2^0) displays sharp and well-resolved peaks. The frequencies agree very well with those expected for a 6cLS configuration (Table 1).[3] In contrast to SCC, the band-fitting analysis reveals no asymmetric peaks, implying that LM2^0 exists only in one conformational state, which is in line with the results of a previous RR study of oligomeric LM2 (Hildebrandt et al., 1989a). Binding of benzphetamine (BP) leads to the appearance of a new peak at 1485.9 cm^{-1} corresponding to the ν_3 mode of a HS configuration. All other marker bands remain largely unchanged except for an intensity increase of the 1562-cm^{-1} band. This indicates that besides the ν_3 mode other modes of the HS species do not significantly contribute to the RR spectrum. The intensification of the 1562-cm^{-1} band may be due to a small contribution of the ν_2 mode of the HS species expected at ~1565 cm^{-1}. There is also no significant effect on the vinyl modes upon BP binding. In an earlier study (Hildebrandt et al., 1989a), an intensity decrease of the high-frequency component has been reported, which is not confirmed by the present data. The previous spectra, however, were measured with lower resolution and larger step widths, which may account for this discrepancy. The shift of the spin equilibrium which is caused by BP binding can be determined quantitatively by using the Raman bands of glycerol as an internal standard to which the RR intensities of LM2 are referenced. The content of the 6cLS configuration in LM2-(BP), α_{6cLS}, is given by

$$\alpha_{6cLS} = \frac{I(\nu_3,\mathrm{LM2[BP]})100}{I(\nu_3,\mathrm{LM2^0})} \qquad (8)$$

where $I(\nu_3,\mathrm{LM2[BP]})$ and $I(\nu_3,\mathrm{LM2^0})$ are the intensities of the ν_3 modes of the 6cLS form in the BP-bound and in the substrate-free LM2. From four different samples an average value for α_{6cLS} of 72% (±1%) was obtained. It should be mentioned that this value refers to a complete saturation of the binding sites. A further increase of the BP concentration does not further lower the 6cLS content.

In the low-frequency region (Figure 7) only minor spectral differences between LM2^0 and LM2(BP) are noted, such as

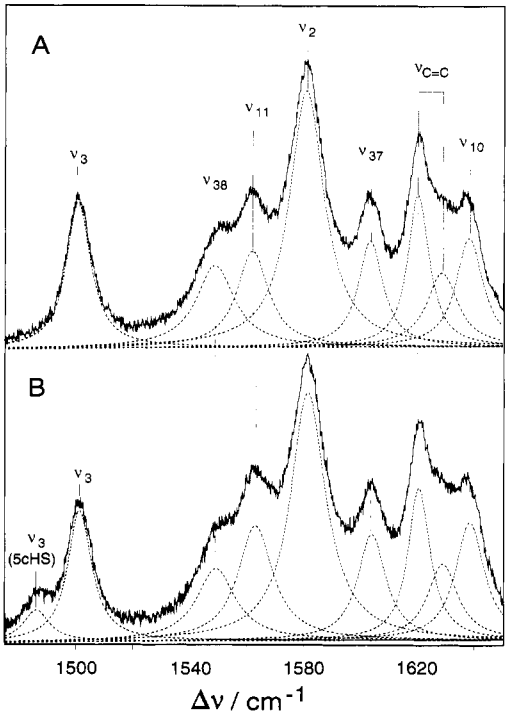

FIGURE 6: High-frequency RR spectra of the oligomeric substrate-free LM2 (A) and the benzphetamine-bound state (B). The spectra were measured at pH 7.25 (150 mM phosphate buffer) at 22 °C in the presence of glycerol. The Raman band of glycerol was subtracted. The dotted lines represent the fitted Lorentzian line shapes.

[3] In a previous RR study of LM2 (Hildebrandt et al., 1989a,b) the reported frequencies were slightly lower due to a calibration error.

Table 6: Comparison of Spin State Marker Band Frequencies of SCC, LM2, and Model Compounds

mode	LM2, 6cLS[a]	SCC, 6cLS[b] state A	SCC, 6cLS[b] state B	PPIX[a] 6cLS	SCC, HS[b] state A	PPIX[a] 6cHS	PPIX[a] 5cHS
ν_3	1500.3	1500.5	1503.6	1502 (+2)	1484.5	1480 (+3)	1491 (+3)
ν_{38}	1550.0	1545.5	1543.8	1554 (+7)	1527.5	1518 (–4)	1533 (–1)
ν_{11}	1557.6	1558.2	1564.2	1562 (–3)	1560.9	1454 (±0)	1553 (–1)
ν_2	1581.7	1582.7	1580.5	1579 (±0)	1568.0	1559 (–2)	1570 (+1)
ν_{37}	1602.2	1601.6	1595.5	1602 (+1)	1583.2	1580 (±0)	1591 (+1)
ν_{10}	1636.9	1637.6	1637.2	1640 (+1)	1602.9	1610 (+3)	1621 (+4)
core size[c]	1.987	1.991	1.991	1.987 (–0.002)	2.028	2.045 (±0.0)	2.016 (–0.003)

[a] Data are taken from Partharasathi et al. (1987); PPIX refers to ferric protoporphyrin IX in the 6cLS (bis-imidazole), 6cHS (bis-DMSO), and 5cHS (chloride) configurations. The values in parentheses give the deviations from the calculated data using the linear core-size frequency relationships. [b] Frequencies (in centimeters^{-1}) are taken from Table 1. [c] Porphyrin core size (in angstroms) calculated from the RR frequencies according to Partharasathi et al. (1987). Values in parentheses give the deviations from experimental (X-ray structure) values [references given by Partarasathi et al. (1987)].

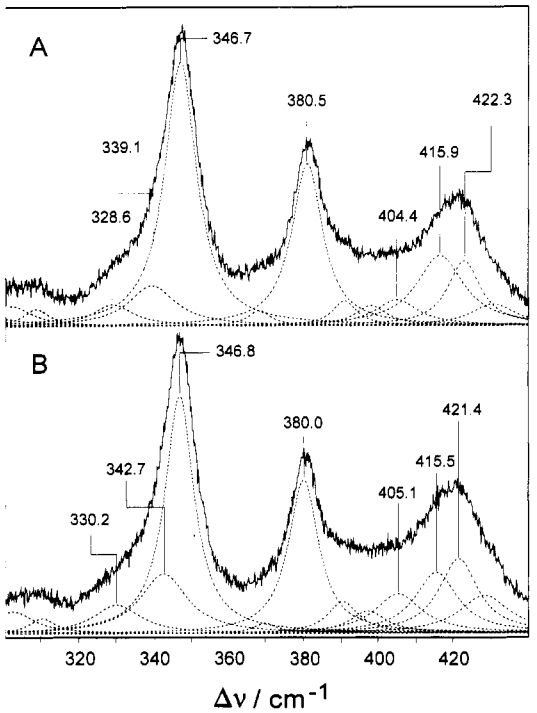

FIGURE 7: Low-frequency RR spectra of the oligomeric substrate-free LM2 (A) and the benzphetamine-bound state (B). The spectra were measured at pH 7.25 (150 mM phosphate buffer) at 22 °C in the presence of glycerol. The Raman bands of glycerol were subtracted. The dotted lines represent the fitted Lorentzian line shapes.

subtle frequency shifts for some of the bands (Table 5) and a small intensity increase of the bands between 400 and 430 cm^{-1}. This is not surprising since, as we showed for SCC (see above), the contribution of the HS form to the low-frequency RR spectrum is much smaller than to the marker band region.

DISCUSSION

Substrate-Free State of SCC and LM2. The prevailing spin configuration in the substrate-free SCC and LM2 is the 6cLS configuragion, confirming previous results obtained for these proteins (Ozaki et al., 1978; Tsubaki et al., 1986; Hildebrandt et al., 1989a,b).[4] In this work, however, it is shown for the first time that SCC^0 exists in two 6cLS forms (states A and B), although the relative contribution of state B to the RR spectrum is smaller due to the lower RR cross sections of the vibrational bands. In contrast to SCC^0 there is not indication for multiple conformational states in LM2^0, although we note slightly larger bandwidths for most of the porphyrin modes compared to SCC^0.

In each case the RR band frequencies reveal a good agreement with those measured for the 6cLS ferric protoporphyrin IX (PPIX), ruling out major distortions of the porphyrin geometry imposed by the protein environment in SCC^0 and LM2^0 (Table 6; Parthrasathi et al., 1987). The only notable differences refer to the mode ν_{38}, which in both 6cLS forms of SCC^0 is lower than in PPIX(6cLS) but close to the value calculated from the linear core size frequency relationship. Such correlations have been derived for each porphyrin mode in this region from the RR spectra of a large number of different metalloprotoporphyrin model compounds and their X-ray structure data (Partharasathi et al., 1987) and, hence, can also be used to calculate the porphyrin core size of the 6cLS hemes of SCC^0 and LM2^0 from the experimental RR frequencies. One obtains 1.991 Å for both state A and B of SCC^0 and 1.987 Å for LM2^0, which both compare very well with the experimental value for 6cLS PPIX (1.989 Å; Table 6).

For cytochrome P-450 (camphor) from *Pseudomonas putida* (CAM) and for the hemoprotein domain of cytochrome P-450 BM-3 from *Bacillus megaterium* (BM-3), the three-dimensional structures have been determined and thus the axial ligands of the heme have been unambiguously identified (Poulos et al., 1986, 1987; Raag & Poulos, 1992; Ravichandran et al., 1993). While a thiolate (cysteine) serves as the fifth ligand, the distal coordination site is oocupied by a water molecule or a hydroxide. Coordination by a hydroxide would readily account for the formation of the 6cLS form. Most likely, this ligation pattern is a general structural motif for all members of the cytochrome P-450 family and, hence, is also valid for the 6cLS forms of SCC^0 and LM2^0.

Substrate Binding to LM2 and SCC. The different response of SCC toward binding of cholesterol and 22*R*-hydroxycholesterol has already been noted in other research groups, who assigned the spin configurations in SCC(chol) and SCC(22R) to 6cHS and 6cLS states, respectively (Shimizu et al., 1981; Tsubaki et al., 1986, 1987). However, as demonstrated in this work, the situation is more complicated due to the conformational equilibrium between the states A and B. Cholesterol binding leads to the formation of the HS species of state B and particularly of state A. While the HS configuration of state B can unambiguously be assigned to a pentaccordinated species, the situation is less clear for the HS form of state A. In ferric HS hemes the frequencies of the marker bands are generally higher by about ~10 cm^{-1} in the pentacoordinated compared to the hexacoordinated state since in the absence of a sixth ligand the iron moves out of the porphyrin plane so that the steric interactions between the HS iron and the pyrrole nitrogens are reduced (Partharasathi

[4] The small amount of the HS forms of state A and B in SCC^0 may be due to residual bound endogeneous cholesterol.

et al., 1987). Thus, the porphyrin geometry can relax to a less stressed conformation. According to the core size frequency relationships, the marker band frequencies of the HS form of state A would correspond to a core size of 2.028 Å, which is just between the values determined for a 6cHS (2.045 Å) and a 5cHS configuration (2.019 Å; Table 6). Thus, it is concluded that in this species a sixth ligand is only weakly bound to the heme iron so that it is slightly displaced out of the plane toward the fifth strongly bound thiolate ligand. Again, the crystal structure data of bacterial cytochromes P-450 provide a plausible explanation (Poulos et al., 1986, 1987; Raag & Poulos, 1992; Ravichandran et al., 1993). In these enzymes the substrate-binding site is located on the distal side of the heme above the pyrrole rings III and IV which carry the propionate groups. Probably, this picture is also valid for SCC and LM2, although it may be that it is ring IV rather than ring III which constitutes the substrate pocket (Tuck et al., 1992). Occupation of the binding pocket by a substrate most likely causes repulsive interaction with the distal ligand of the heme iron. In this way, the axial bond of the hydroxide to the iron may be weakened so that the iron moves out of the porphyrin plane toward the thiolate ligand.

In LM2, benzphetamine binding causes a partial (28%) transition to a HS configuration. The only detectable marker band of this HS form is the mode ν_3 at 1485.9 cm^{-1}, which is very close to the value of the ν_3 mode of the HS form of state A in SCC(chol). Thus it is very likely that there is a comparably weak interaction with the distal water ligand for both HS species.

In this context it is interesting to recall that in reconstituted systems the benzphetamine-bound LM2 HS content is significantly larger than in solubilized LM2 oligomers and the mode ν_3 at 1488 cm^{-1} is much closer to the expected value for a 5cHS than for a 6cHS configuration (Hildebrandt et al., 1988). Similar results were obtained for the complex of phenyloctane and solubilized LM2 (Hildebrandt et al., 1989b). On the other hand, binding of benzphetamine to the monomeric enzyme does not produce any HS at all (Hilderbrandt et al., 1989a). These findings suggest that protein–protein interactions as well as the kind of substrate sensitively control the degree of HS formation and the actual coordination geometry on the distal side of the heme.

Even taking into account such an intermediate core size for the HS form of state A in SCC(chol), there are still significant deviations between the measured and the calculated frequencies for the modes ν_{11} and ν_{10} (Table 6), which reflect the specific interactions between the heme and the protein environment and/or the bound cholesterol. If such interactions caused a ruffling of the porphyrin geometry, they would be reflected by a downshift not only of ν_{10} but also of ν_{11}, ν_2, and ν_3 (Alden et al., 1989; Czernuszewicz et al., 1989; Shelnutt et al., 1991), which, however, is not observed. Alteration of the electron density distribution in the porphyrin due to inductive effects via the conjugated substituents or due to π back donation have been shown to cause both positive and negative deviations of the various modes and among them ν_{11} is a particularily sensitive mode in this respect (Partharasathi et al., 1987; Anzenbacher et al., 1989). However, the upshift of this mode would imply a reduced electron density of the porphyrin π orbitals which is not very likely, taking into account the strong electron-donating capacity of the thiolate ligand (Ozaki et al., 1978; Jung et al., 1983, 1992; Lange et al., 1994).

On the other hand, we would like to recall that in monomeric LM2 the mode ν_{11} responds to benzphetamine binding (Hildebrandt et al., 1989a). Taking into account that this mode is, to a major extent, localized in the pyrrole rings III and IV (Lee et al., 1986), which constitute a part of the substrate binding pocket (Poulos et al., 1986, 1987), the spectral changes associated with ν_{11} have been ascribed to direct interactions between the porphyrin and the bound benzphetamine (Hildebrandt et al., 1989a). We suggest that the same type of interaction is responsible for the unusual frequency upshift of this mode in the 6cHS form of SCC-(chol). Specific substrate–heme interactions have also been inferred from other studies of cytochromes P-450 employing different techniques (Orme-Johnson et al., 1979; Larroque et al., 1990).

The most likely candidate for the sixth ligand in the 6cHS form of state A is a water molecule. This implies that the transition between the 6cHS and the 6cLS form of state A is initiated by a proton transfer step and the spin equilibrium is strongly pH-dependent. This is in fact observed (Table 6). The spin equilibrium constant of state A decreases by a factor of $\sim$8 upon increasing the pH from 7.4 to 8.4. In contrast, the spin equilibrium constant of state B only reveals a moderate decrease by a factor of $\sim$1.4. These results are in line with those obtained by Lange et al. (1992a), although the data provided by these authors were obtained in the presence of ethylene glycol at –20 and 22 °C for states A and B, respectively.

The formation of the 6cHS configuration in the SCC(chol) implies that the occupation of the substrate binding site by cholesterol favors the protonation of the hydroxide ligand. This is not surprising since a large hydrophobic molecule such as cholesterol is expected to lower the effective dielectric constant in its immediate vicinity, which, in turn, would shift acid–base equilibria toward the neutral forms, i.e., from hydroxide to water.

In contrast to the cholesterol, binding of 22*R*-hydroxycholesterol does not change the spin configuration; i.e., the complex is essentially 6cLS although an increase of the LS species of state A relative to state B is noted (Table 3). It is reasonable to assume that the hydroxyl group of this substrate is located close to the heme iron (Tsubaki et al., 1987). Hence, it may be that the C-22 hydroxyl group stabilizes the axial hydroxyl ligand, i.e., the 6cLS configuration, or alternatively, directly interacts with the heme iron, serving itself as the sixth ligand in this 6cLS form of the SCC(22R) complex.

The spectral differences between the 6cLS forms of state A of SCC^0, SCC(chol), and SCC(22R) may reflect the interactions of the substrate with the porphyrin and, in the case of SCC(22R), a possible change of sixth axial ligand. The modes ν_{38}, ν_{11}, and ν_2 are significantly broadened upon substrate-binding, while the half-widths of ν_{10} and the vinyl stretching vibrations are strongly reduced (Table 1). This can readily be understood in terms of vibrational energy transfer between the modes of the heme and those of the adjacent molecules (Hildebrandt & Stockburger, 1984; Sassaroli et al., 1989; Hildebrandt et al., 1993). In the substrate-free state, the substrate binding pocket is probably largely occupied by water molecules (Jacobs et al., 1987) which exhibit a bending mode at $\sim$1635 cm^{-1}. Hence, porphyrin modes with frequencies in this range are capable of transferring energy to the nearby water molecules, thereby reducing the lifetime of the vibrationally excited state and increasing the half-width of the RR bands. Such modes are the vinyl stretching vibrations and the porphyrin mode ν_{10}. Upon binding of substrates, those solvent molecules are (partly) expelled from the substrate binding pocket so that energy transfer to water is less efficient and the bandwidths of these modes decrease. Instead, in SCC(chol) and SCC(22R) the

substrates themselves may provide potent acceptor modes for vibrational energy transfer from the porphyrin between 1500 and 1600 cm^{-1}, which readily accounts for the broadening of the bands in this region (ν_{38}, ν_{11}, and ν_2) relative to the 6cLS form (A) of SCC^0.

Frequency shifts and intensity changes are observed for some of the porphyrin modes including ν_{11}, the sensitivity of which toward substrate binding has been already discussed in the case of the 6cHS configuration.

The different response of the RR spectrum of SCC to cholesterol and 22*R*-hydroxycholesterol binding is also reflected by the bands in the low-frequency region (Table 5). These modes involve vibrations of the peripheral substituents and, hence, most sensitively indicate differences of the heme–protein interactions (Hildebrandt, 1992). For example, the modes at ~420 and 412 cm^{-1} include significant contributions of the vinyl bending vibrations (Uchida et al., 1988). The frequency upshift and narrowing of the latter band and the concomitant intensity decrease in SCC(22R) as compared to SCC(chol) point to a conformational change of one of these substituents. On the other hand, the 420-cm^{-1} band remains unchanged. This is in agreement with the behavior of the stretching vibrations of these substituents (Table 1). The lower frequency component at 1617 cm^{-1} exhibits a similar frequency, half-width, and intensity in both complexes while the higher frequency component is significantly narrower (as the bending mode at ~412 cm^{-1}) and downshifted in SCC-(22R).

Conformational Equilibria and Substrate Binding. The transition between the conformational states A and B involves structural changes in the protein including the amide backbone as indicated by the CD spectra (Lange et al., 1992b). The structural changes also extend to the heme pocket causing different coordination configurations of the HS forms of state B (5cHS) and state A (6cHS). Structural differences between states A and B are also reflected by the RR spectra of the 6cLS species of SCC(chol). There are notable changes of the frequencies and relative intensities of most of the porphyrin modes, implying differences in the ground-state conformation of the porphyrin due to structural alterations of the heme pocket (Table 1). Apparently, these changes particularly refer to the vicinity of the vinyl substituents. While in state A the low-frequency component of the vinyl stretching mode is of a comparable intensity as the high-frequency component, a drastic intensity redistribution as well as distinct frequency upshifts are noted in state B. Furthermore, state B exhibits markedly lower frequencies for the E_u modes ν_{37} and ν_{38}, associated with a strong intensity increase, and a substantially higher frequency of mode ν_{11}. The underlying molecular origin of these differences is not clear, although it is reasonable to assume that in particular the shift of ν_{11} may reflect structural differences of the substrate binding pocket and/or substrate–heme interactions as discussed above.

In this context it is interesting to refer to a recent study by Tsubaki et al. (1992). These authors have studied the C=O stretching vibrations of the carbon monoxide complexes of the substrate-binding SCC and observed two IR bands in SCC(22R) but only one in the case of cholesterol or other substrates. The appearance of two bands in SCC(22R) was interpreted in terms of a productive and a nonproductive binding configuration. It is tempting to relate these configurations to the conformational states A and B analyzed in this work. This would imply a significant change of the conformational equilibrium upon 22R binding, which is, however, not observed (Tables 3 and 4). Within the experimental accuracy, the content of state A (6cLS and 6cHS) as determined by the RR spectra is largely the same in SCC^0, SCC(22R), and SCC(chol).

Structural Heterogeneity in SCC and LM2. The crystal structure of the heme protein domain BM-3, which has recently been determined by Ravichandran et al. (1993), may provide a key for the understanding of the structural heterogeneity in SCC. These authors have concluded that the substrate-binding pocket of this enzyme may adopt various conformations, which is in sharp contrast to CAM (Raag & Poulos, 1992; Poulos et al., 1986). These differences may be related to the larger size of the natural substrates of BM-3 (long-chain fatty acids) as compared to those of CAM, so that a higher structural flexibility of the substrate-binding pocket is required to accommodate the substrates. The same considerations may hold for SCC and the sterically demanding steroid substrates. The structural differences between states A and B of SCC include the ligation pattern and the geometry of the heme as well as its interactions with the immediate protein environment, i.e, the active site and the substrate binding pocket. The two conformational states of SCC which have been characterized by RR spectroscopy represent the minimum number of conformers required to interpret the experimental data; however, we cannot rule out that there are further conformational states which are not distinguishable on the basis of the RR spectra.

On the basis of the high amino acid sequence agreement and the functional similarity, Ravichandran et al. (1993) have concluded that the crystal structure of BM-3 may represent a better model for microsomal enzymes than CAM. In fact, also in the case of LM2 a conformational heterogeneity of the protein has been demonstrated, however, only at temperatures above 32 °C and in (reconstituted) membrane systems (Krüger, 1992). The dynamics of this heterogeneity, apparently intimately related with the oligomeric structure of LM2, may be important for allosterism and cooperativity in control of its enzymic function (Stier et al., 1991a,b). On the other hand, at ambient temperature and in the solubilized state, the RR spectra of LM2 oligomers do not provide any evidence for multiple conformers. Moreover, previous RR data of LM2 monomers and oligomers in the substrate-free and substrate-bound state have revealed only small spectral differences (Hildebrandt et al., 1989b), which are by far not so pronounced as those between the conformers in SCC. Consequently, we conclude that, at least at ambient temperature, the protein structure of SCC must be more flexible than LM2, in particular, in the vicinity of the heme pocket, which may be related to the different size of the specific substrates as discussed above.

The present study provides insight into the intrinsic conformational heterogeneity of the active sites of SCC and LM2, which may be of relevance for the substrate specificity as well as for the proper course of the catalytic processes in these enzymes. However, it is necessary to point out that under physiological conditions lipid–protein and protein–protein interactions may sensitively control the conformational equilibria of these enzymes (Akhrem et al., 1979; 1985; Stier et al., 1988, 1991a,b; Schwarz et al., 1993).

Finally, we wish to point out that the results obtained for SCC and LM2 are also of interest within the concept of conformational substrates of proteins and enzymes in general [cf. Frauenfelder et al. (1991)]. A detailed structural analysis of such substates may provide the key for understanding the molecular mechanisms of biochemical and biophysical processes.

ACKNOWLEDGMENT

We gratefully acknowledge the active and generous support of Professor Kurt Schaffner.

REFERENCES

Abe, M., Kitagawa, T., & Kyogoku, Y. (1978) *J. Chem. Phys. 69*, 4526–4534.

Akhrem, A. A., Lapko, V. N., Lapko, A. G., Shkumatov, V. M., & Chashchin, V. L. (1979) *Acta Biol. Med. Ger. 38*, 257–273.

Akhrem, A. A., Adamovich, T. B., Lapko, V. N., Sherman, S. A., Usanov, S. A., Shkumatov, V. M., & Chashchin, V. L. (1985) *Dev. Biochem. 27*, 113–119.

Alden, R. G., Crawford, B. A., Doolen, R., Ondrias, M. R., & Shelnutt, J. A. (1989) *J. Am. Chem. Soc. 111*, 2070–2072.

Anzenbacher, P., Evangelista-Kirkup, R., Schenkman, J., & Spiro, T. G. (1989) *Inorg. Chem. 28*, 4491–4495.

Backes, W. L., Tamburini, P. P., Jansson, I., Gibson, G. G., Sligar, S. G., & Schenkman, J. B. (1985) *Biochemistry 24*, 5130–5136.

Cinti, D. L., Sligar, S. G., Gibson, G. G., & Schenkman, J. B. (1979) *Biochemistry 18*, 36–42.

Czernuszewicz, R. S., Li, X.-Y., & Spiro, T. G. (1989) *J. Am. Chem. Soc. 111*, 7024–7031.

Frauenfelder, H., Sligar, S. G., & Wolynes, P. G. (1991) *Science 254*, 1598–1603.

Heibel, G. E., Hildebrandt, P., Ludwig, B., Steinrücke, P., Soulimane, T., & Buse, G. (1993) *Biochemistry 32*, 10866–10877.

Heinzelmann, R. V., & Aspergren, B. D. (1957) U.S. Patent 2789138.

Hildebrandt, P. (1992) in *Frontiers in Biotransformation* (Ruckpaul, K., & Rein, H., Eds.) pp 166–215, Akademie-Verlag, Berlin.

Hildebrandt, P., & Stockburger, M. (1984) *Biochemistry 23*, 5539–5548.

Hildebrandt, P., Greinert, R., Stier, A., Stockburger, M., & Taniguchi, H. (1988) *FEBS Lett. 227*, 76–80.

Hildebrandt, P., Greinert, R., Stier, A., & Taniguchi, H. (1989a) *Eur. J. Biochem. 186*, 291–302.

Hildebrandt, P., Garda, H., Stier, A., Bachmanova, G. I., Kanaeva, I. P., & Archakov, A. I. (1989b) *Eur. J. Biochem. 186*, 383–388.

Hildebrandt, P., Heimburg, T., & Marsh, D. (1990) *Eur. J. Biophys. 18*, 193–201.

Hildebrandt, P., Vanhecke, F., Heibel, G., & Mauk, A. G. (1993) *Biochemistry 32*, 14158–14164.

Imai, Y., Hashimoto-Yutsudo, C., Satake, H., Girardin, A., & Sato, R. (1980) *J. Biochem. (Tokyo) 88*, 489–503.

Jacobs, R. E., Singh, J., & Vickery, L. E. (1987) *Biochemistry 26*, 4541–4545.

Jung, C., Ristau, O., & Jung, C. (1983) *Theor. Chim. Acta 63*, 143–159.

Jung, C., Hui Bon Hoa, G., Schröder, K. L., Simon, M., & Doucet, J. P. (1992) *Biochemistry 31*, 12855–12862.

Kitagawa, T., & Ozaki, Y. (1987) *Struct. Bond. 64*, 71–114.

Krüger, V. (1992) Ph.D. Thesis, Universität Göttingen.

Lange, R., Maurin, L., Larroque, C., & Bienvenüe, A. (1988) *Eur. J. Biochem. 172*, 189–195.

Lange, R., Larroque, C., & Anzenbacher, P. (1992a) *Eur. J. Biochem. 207*, 69–73.

Lange, R., Pantaloni, A., & Saldana, J.-L. (1992b) *Eur. J. Biochem. 207*, 75–79.

Lange, R., Heiber-Langer, I., Bonfils, C., Fabre, I., Negishi, M., & Balny, C. (1994) *Biophys. J. 66*, 89–98.

Larroque, C., & Van Lier, J. E. (1986) *J. Biol. Chem. 261*, 1083–1087.

Larroque, C., Lange, R., Maurin, L., Bienvenüe, A., & Van Lier, J. E. (1990) *Arch. Biochem. Biophys. 282*, 198–201.

Lee, H., Kitagawa, T., Abe, M., Pandey, R. K., Leung, H.-K., & Smith, K. M. (1986) *J. Mol. Struct. 146*, 329–347.

Nelson, D. R., Kamataki, T., Waxman, D. J., Guengerich, F. P., Estabrook, R. W., Feyereisen, R., Gonzales, F. J., Coon, M. J., Gunsalus, I. C., Gotoh, O., Okuda, K., & Nebert, D. W. (1993) *DNA Cell Biol. 12*, 1–51.

Orme-Johnson, N. R., Light, D. R., White-Stevens, R. W., & Orme-Johnson, W. H. (1979) *J. Biol. Chem. 254*, 2103–2111.

Ortiz de Montellano, P. R., Ed. (1986) *Cytochrome P-450: Structure, Mechanism, and Biochemistry*, Plenum Press, London.

Ozaki, Y., Kitagawa, T., Kyogoku, Y., Imai, Y., Hashimoto-Yutsudo, C., & Sato, R. (1978) *Biochemistry 17*, 5826–5831.

Partharasathi, N., Hansen, C., Yamaguchi, S., & Spiro, T. G. (1987) *J. Am. Chem. Soc. 109*, 3865–3871.

Poulos, T. L., Finzel, B. C., & Howard, A. J. (1986) *Biochemistry 25*, 5314–5322.

Poulos, T. L., Finzel, B. C., & Howard, A. J. (1987) *J. Biol. Chem. 195*, 687–700.

Raag, R., & Poulos, T. L. (1992) in *Frontiers in Biotransformation* (Ruckpaul, K., & Rein, H., Eds.) pp 1–43, Akademie-Verlag, Berlin.

Ravichandran, K. G., Boddupalli, S. S., Hasemann, C. A., Peterson, J. A., & Deisenhofer, J. (1993) *Science 261*, 731–736.

Rein, H., Jung, C., Ristau, O., & Friedrich, J. (1984) in *Cytochrome P-450* (Ruckpaul, K., & Rein, H., Eds.) pp 163–249, Akademie-Verlag, Berlin.

Ruckpaul, K., & Rein, H., Eds. (1984) *Cytochrome P-450*, Akademie-Verlag, Berlin.

Sassaroli, M., Cing, Y.-C., Dasgupta, S., & Rousseau, D. L. (1989) *Biochemistry 28*, 3128–3132.

Schuster, I., Ed. (1989) *Cytochrome P-450: Biochemistry and Biophysics*, Taylor & Francis, London.

Schwarz, D., Krüger, V., Chernogolov, A. A., Usanov, S. A., & Stier, A. (1993) *Biochem. Biophys. Res. Commun. 195*, 889–896.

Shelnutt, J. A., Medforth, J. C., Berber, M. D., Barkigia, K. M., & Smith, K. M. (1991) *J. Am. Chem. Soc. 113*, 4077–4087.

Shimizu, T., Kitagawa, T., Mitani, F., Iizuka, T., & Ishimura, Y. (1981) *Biochim. Biophys. Acta 670*, 236–242.

Sligar, S. G., & Gunsalus, I. C. (1979) *Biochemistry 18*, 2290–2295.

Spiro, T. G., Ed. (1988) *Biological Applications of Raman Spectroscopy*, Vol. 3, Wiley, New York.

Stier, A., Krüger, V., Eisbein, T., & Finch, S. A. E. (1991a) in *Molecular Aspect of Monooxygenases and Bioactivation of Toxic Compounds* (Arnc, E., Schenkman, J. E., & Hodgson, E., Eds.) pp 93–113, Plenum, New York.

Stier, A., Krüger, V., Eisbein, T., & Finch, S. A. E. (1991b) in *Molecular Aspect of Monooxygenases and Bioactivation of Toxic Compounds* (Arnc, E., Schenkman, J. E., & Hodgson, E., Eds.) pp 115–133, Plenum, New York.

Suhara, K., Takemori, S., & Katagiri, M. (1972a) *Biochim. Biophys. Acta 263*, 272–278.

Suhara, K., Ikeda, Y., Takemori, S., & Katagiri, M. (1972b) *FEBS Lett. 28*, 45–47.

Suhara, K., Gomi, T., Sato, H., Itagaki, E., Takemori, S., & Katagiri, M. (1978) *Arch. Biochem. Biophys. 190*, 290–299.

Tsubaki, M., Hiwatashi, A., & Ichikawa, Y. (1986) *Biochemistry 25*, 3563–3569.

Tsubaki, M., Hiwatashi, A., & Ichikawa, Y. (1987) *Biochemistry 26*, 4535–4540.

Tsubaki, M., Yoshikawa, S., Ichikawa, Y., & Yu, N.-T. (1992) *Biochemistry 31*, 8991–8999.

Tuck, S. F., Peterson, J. A., & Ortiz de Montellano, P. R. (1992) *J. Biol. Chem. 267*, 5614–5620.

Uchida, K., Susai, Y., Hirotani, E., Kimura, T., Yoneya, T., Takeuchi, H., & Harada, I. (1988) *J. Biochem. (Tokyo) 103*, 979–985.